



Corrosion Inhibition Efficiency of Polyvinylpyrrolidone-Cysteine on Mild Steel in 1.0 M HCl Solution

Craig. K. Nsakabwe¹ · Mamookho E. Makhatha¹ · George M. Tsoeunyane¹ · Akinsanya D. Baruwa¹

Received: 6 December 2021 / Revised: 21 January 2022 / Accepted: 14 February 2022 / Published online: 25 February 2022
© The Author(s), under exclusive licence to Springer Nature Switzerland AG 2022

Abstract

In this work, the inhibitive capability of Cysteine-doped Polyvinylpyrrolidone (PVPC) in 1.0 M HCl solution was investigated using mild steel as the reference material. To elucidate the effect of concentration on the corrosion inhibition efficiency, the synthesized PVPC via solution polymerization method was added to the acidic solution at different optimized concentrations of 25, 100, 300, 500, and 700 ppm and were characterized. Fourier-transformed infrared (FTIR), X-ray diffractometer (XRD), and scanning electron microscope equipped with energy dispersive spectroscopy (SEM/EDX) were used to study the bonding, phase formation, morphology, and elemental composition of the polymeric surface, while gravimetric analysis techniques were used to determine the corrosion rate. The C–H functional group dominance in the FTIR spectra indicated adequate surface adsorption of PVPC. It further reflected that cysteine concentration does not affect the molecular bond and intrinsic characteristics. The XRD pattern of PVPC showed mixed amorphous and crystalline structures because of different characteristics of Polyvinylpyrrolidone and Cysteine. The SEM/EDX analysis indicated that the increase in concentration caused changes in the composites' surface morphologies and resultant chemical compositions. It, however, displayed the maximum inhibition efficiency of 97% at 700 ppm. From the Langmuir isotherm model, kinetic and thermodynamic values suggested that both competitive physisorption and chemisorption processes occurred. However, physisorption was established as the predominant phenomenon during the physicochemical adsorption mechanism.

Keywords Concentration · Cysteine · Mild steel · Polyvinylpyrrolidone · Inhibition efficiency

1 Introduction

Mild steel (MS) is regarded as a critical material due to its excellent mechanical properties and relative affordability. It is used for various applications, including construction, machinery parts, and pipelines [1–3]. Despite its application in many sectors, mild steel remains highly susceptible to corrosion when exposed to a harsh environment. Its corrosion is most experienced during acid cleaning, pickling, descaling, and drilling in oil and gas exploration [4, 5]. These operations use acidic solutions extensively and expose the steel-made vessels or surfaces to corrosion [6–9].

Due to corrosion failure, huge financial, energy, and human resources losses are recorded yearly. It is estimated that failure due to corrosion is around 3% of the world's GDP (Reference is from NACE data). Different techniques have been proposed and used to prevent or mitigate corrosion loss [10]. These include cathodic and/or anodic protection, coating, alloying elements, and the use of corrosion inhibitors are mostly considered the most efficient and confident ways to address corrosion problems [11, 12]. Cathodic protection exhibited great usefulness in the treatment of embedded or buried metals, the uncertainty of the lifespan of anodes causes a major concern to its applicability [13]. Alloying has improved steel corrosion resistance, but the reinforcement's intermetallic compound formation and spinodal decomposition at elevated temperatures limit its application [14]. Coating proved to be very efficient and easy to maintain. However, non-organic coatings pose health and environmental challenges [15].

Due to green processes [16–18] and environmental constraints placed on inorganic inhibitors, organic inhibitors

✉ Mamookho E. Makhatha
emakhatha@uj.ac.za

✉ Akinsanya D. Baruwa
darebaruwa@gmail.com

¹ Department of Metallurgy, Faculty of Engineering and the Built Environment, University of Johannesburg, Johannesburg, South Africa

have received significant attention [19, 20]. Organic inhibitors possess a relatively high solubility in aqueous media and simple adsorption onto the metal surface, forming a stable inhibitive layer [21]. Organic coatings such as poly(aniline-anisidine) doped with chitosan and SiO_2 have proven to improve the resistance of mild steel to rapid corrosion occurrence in the marine environment [22]. Furthermore, the polymeric inhibitors have also displayed good corrosion inhibition because their molecular configuration offers adhesion and bonding properties [23, 24]. Researchers such as Abdel Hamed et al. [25, 26] have worked extensively using expired drugs to control the rate at which corrosion occurs. However, mitigating corrosion of metals such as mild steel has been a tough challenge and still a menace. Using either organic or inorganic compounds for surface coating has been researched extensively and has shown their pros and cons. However, the hybridization of organic–inorganic compounds for corrosion prevention has not been effectively established in process, availability, and cost [27].

As one of the polymeric corrosion inhibitors, Polyvinylpyrrolidone (PVP) has several advantages, including high biodegradability, excellent solubility in organic solvents, good spinnability, and the ability to interact with other compounds [28, 29]. Other characteristics such as availability, biocompatibility, non-toxicity, inert, and pH stability make the polymer worthy of investigation and applicable [30]. In addition, PVP was reported as a mixed-type corrosion inhibitor [31] and had a relatively weaker inhibition efficiency in its actual state. This deficiency discourages its acceptance as the sole inhibitor. Although many green and organic inhibitors do have mixed-type corrosion [32–34], the efficiency of inhibitors such as PVP can be improved by increasing the concentration within an electrolyte or combining some additives [31, 35]. This process could eventually lead to a higher electrolyte viscosity that could hinder the transfer of the polymer chain from the electrolyte to the metal surface, rendering a complex inhibition process [28, 29]. The other challenge faced when increasing the concentration of inhibitors such as PVP is the high cost. However, lowering the concentration of inhibitors usually results in a lack of active agents at the metal–solution interface. Because of these instances, the optimum inhibitor concentration should always be considered for efficient and cost-effective corrosion control. Effective synthesis of PVP could be an advantage to mitigate the concentration dilemma.

Therefore, this current study attempts to evaluate the effect of cysteine concentrations on the readily available polyvinylpyrrolidone complex to improve the PVP's weak

protection efficiency on mild steel when exposed to a harsh environment. Cysteine has proven to be a tremendous competitive inhibitor by the nature of its catalytic activity. It could function irreversibly to form either temporary or permanent inactivation activity [36]. Harnessing the individual characteristics of both compounds will contribute to inhibiting corrosion occurrence associated with mild steel.

2 Experimental Procedure

2.1 Materials

Analytical grade polyvinylpyrrolidone (PVP), cysteine, oxalic acid, ammonium persulfate ($\text{NH}_4\text{S}_2\text{O}_8$), ammonium hydroxide solution (NH_4OH), hydrochloric acid (HCl 32%), and acetone ($(\text{CH}_3)_2\text{CO}$) were purchased from Sigma Aldrich. The mild steel (MS) specimen was provided by a local South African steel-making company (Metal Centre).

The chemical composition is determined using optical emission spectroscopy (OES). The elemental composition of mild steel is represented in Table 1. The experimental methodology and the stepwise synthesis procedure are illustrated in Fig. 1a and b.

This investigation was conducted in consecutive steps, as displayed in the flow chart presented in Fig. 1a and synthesis in Fig. 1b. The as-received materials were characterized for chemical and mineral phase contents, surface morphology, and functional group identification in the first step. Next, was the synthesis and polymerization stage, and finally, the addition of inhibitors (with different concentrations) to the electrolyte, followed by other characterizations.

2.2 Synthesis of PVP with Cysteine

For the synthesis, 10 g of polyvinylpyrrolidone (PVP) was dissolved in 100 ml of 0.5 M oxalic acid solution giving a 10% PVP solution. Three different masses of cysteine (C) were weighed and prepared separately for the three ratios of cysteine (1, 3, and 5%) at low pH of 1.3 to make a solution. The two solutions were mixed under a 2:1 ratio with a dominant PVP mass. The mixture was stirred for 2 h using a magnetic stirrer at 1500 rpm before refrigerating within a temperature range of 0–5 °C. 1% $\text{NH}_4\text{S}_2\text{O}_8$ was added dropwise to the mixture, and the pH adjusted to 8–9 by the addition of NH_4OH . The mixture got homogenized at room temperature after being stirred for 3 h using a magnetic stirrer at 1500 rpm. The homogenized mixture was refrigerated

Table 1 Elemental composition of mild steel

Element	C	Mn	P	Cr	Mo	Ni	Al	Cu	Co	Fe
Wt. %	0.06	0.25	0.009	0.04	0.01	0.02	0.05	0.01	0.01	99.3

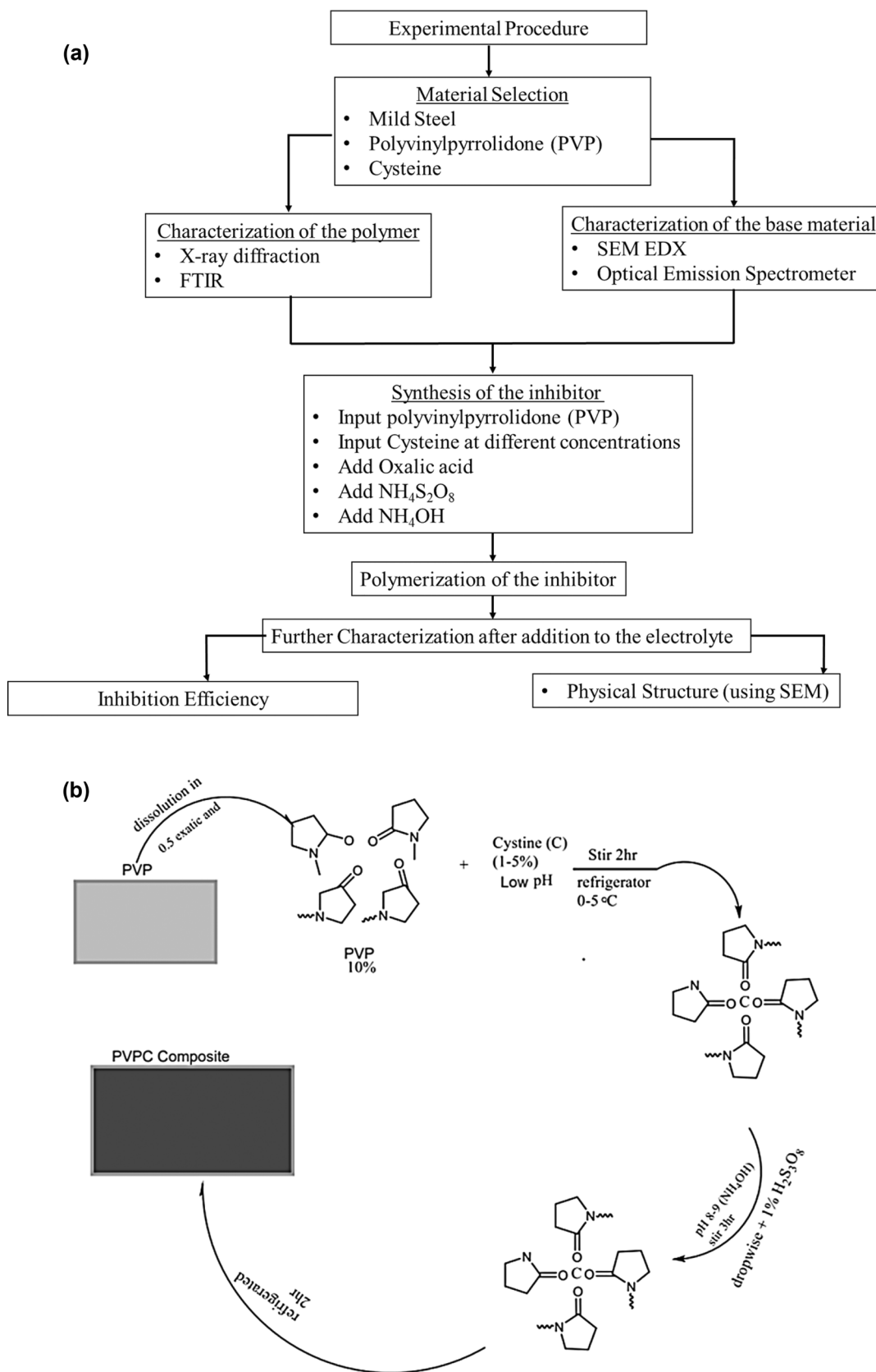


Fig. 1 a The flow chart of the experimentation methodology and b stepwise synthesis procedure

for 24 h within the temperature range of 0–5 °C to initiate the polymerization process. The polymerized blend was precipitated using acetone, filtered, dried, and stored.

Three different ratios (1, 3, and 5%) of cysteine were used to prepare the PVPC polymer composite in which the PVP represented 10% of the total weight. The PVPC mentioned in this section is a blend of polyvinylpyrrolidone (PVP) and cysteine(C).

2.3 Characterization of the Materials and Polymer

The synthesized polymer composites were subjected to characterizations to determine their molecular structure and chemical composition. The following techniques were used for the characterization of the materials.

2.3.1 Morphology and Elemental Composition

- QA4TASMAN Arc-spark Optical Emission Spectrometer (OES) was used for the elemental analysis of the substrate.
- Vega 8 Tescan scanning electron microscope (SEM) equipped with Energy-Dispersive X-ray Spectroscopy (EDX) was utilized to observe the surface morphology. EDX analysis was performed to determine the elemental composition of each of the analysed molecules. The scans were done before and after immersion.

2.3.2 Surface Chemistry and Phase Identification

- Fourier-Transformed Infrared (FTIR) of Nicolet iS10 model was adopted for the functional group identification. The samples were scanned in the range of 400 to 4000 cm^{-1} at the resolution rate of 4 cm^{-1} after 32 scans.
- X-ray Diffraction Rigaku Ultima IV instrument (XRD-PDXL analysis software) determined mineral phase identification. The instrument was operated at 40 kV and 30 mA and with a detection limit of 2%. Data were recorded over the range $5^\circ \leq 2\theta \leq 95^\circ$ at a scan rate of 0.5°/min and step width of 0.01°.

2.3.3 Corrosion Rate and Inhibition Efficiency

The mild steel's corrosion rate (mm/year) was evaluated on well-polished and clean mild steel (MS) specimens of surface area $25 \times 25 \text{ mm}^2$. It was exposed to an uninhibited and inhibited solution (1.0 M HCl) as an aggressive medium. 1000 ppm of PVPC was prepared as a stock solution prior to corrosion tests. The weight-loss method was used to evaluate the corrosion inhibition of the PVPC using Eq. (1).

$$\text{IE} = [1 - (W_2/W_1)] * \quad (1)$$

where IE (%) is the inhibition efficiency, W_1 (g) change in the mass value of the steel exposed to an uninhibited 1.0 M HCl solution, and W_2 (g) is the change in the mass value of mild steel exposed to an inhibited 1.0 M of HCl solution.

Therefore, the corrosion rate is expressed in mm/year and was determined using Eq. (2):

$$\text{CR} = (87.6 * W)/tAd, \quad (2)$$

where CR is the corrosion rate (mm/year), W is the change in mass (g), d is the density of the mild steel, A is the mild steel surface area (mm^2) and t corresponds to the immersion time (h).

3 Results and Discussion

3.1 Sample Characterization

3.1.1 FTIR and XRD Analysis

Figure 2 summarizes the characterization data obtained from the pure PVP, pure cysteine, and PVPC at different concentrations using FTIR and XRD. The figure assesses the physicochemical properties of the synthesized PVPC and compares the composition of each material against the pure PVP.

The FTIR results reveal a similar spectrum shape of PVPC at the various percentage cysteine addition. It could suggest that the cysteine addition had little impact on the intrinsic characteristic of the polymer composite. Furthermore, the molecular bonding is the same for all the three PVPC molecules synthesized from the three considered cysteine ratios. Peak band composition, characteristics, and vibration modes are summarized in Table 2.

The C–H bending and stretching mode prevalence in the spectra indicate successful grafting of inhibitors on the surface of mild steel. The band C–H of pure PVP shifted from 2941.28 to 2974.9 cm^{-1} of the synthesized PVPC [37]. There is a shift in the N–H band from 3266.69 cm^{-1} to lower frequencies of 3186.15 cm^{-1} and 1582 cm^{-1} [38], which could result from wagging H-bonding. It is evident that the synthesized PVP has no vibration for C–O, which is found in pure PVP at 1067.31 cm^{-1} and pure Cysteine at 1139.3 cm^{-1} ; this could have been suppressed by the N–H amide group dominant in the spectrum. N=C=S is found at a wavelength 1421.67 cm^{-1} in PVPC, which emanates from Cysteine's stretch mode.

The XRD patterns of PVP, Cysteine, and PVPC are presented in Fig. 2b. From the XRD plot, the PVP is amorphous (disordered) while the C is crystalline (ordered) in

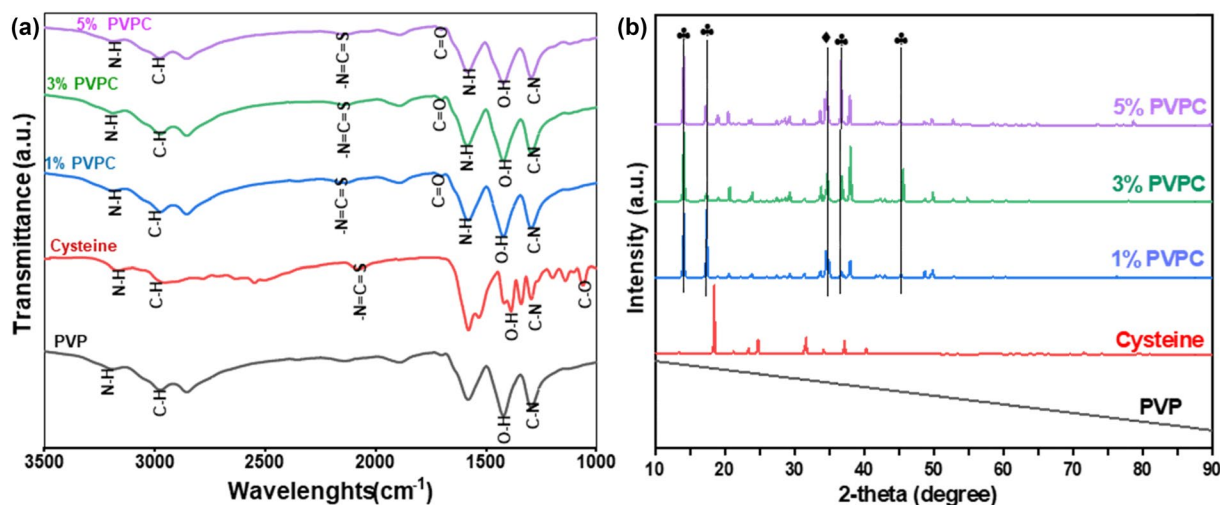


Fig. 2 FTIR (a) and XRD (b) spectra of pure PVP, pure cysteine, and PVPC at different concentrations

Table 2 FTIR transition bonds of PVP, C, and PVPC

Bond stretch	Wave numbers (cm ⁻¹)			Vibration modes
	PVP	C	PVPC	
N-H	3266.69	3165.50	3186.15;1582	Stretching mode
C-H	2941.28	2954.10	2974.90	Bending and stretching mode
C=O	1657.37	1579.00	1699.93	Stretching mode
C-O	1067.31	1139.30	-	Stretching mode
C-N	1274.96	1293.70	1294.97	Stretching mode
-N=C=S	-	2076.80	2147.70	Stretching mode
O-H	1424.59	1389.21	1421.67	Bending mode

nature. PVPC forms sharp peaks due to a transformation in the lattice structure resulting from the filling and bonding of the C. According to Tobyn et al. [39], the corresponding physical mixes produced a diffuse pattern characteristic for a polymer. These phases are at a 2-theta interval of diffraction angles between 10° and 40°. Sharp peaks could be attributed to the presence of the hydrogen bond originating from the interactions between the amorphous phase of PVP with the crystalline phase of Cysteine, as earlier outlined by Tobyn et al. [39]. The doped PVP phase peaks' intensities are reduced compared to the peaks of pure Cysteine, while 3% PVPC shows to be the least affected. However, a broad lump is observed between 2θ equal to 33.4° and 35.3°, which could be associated with an increase in the amorphous domain of PVP polymer and clear diffraction peaks corresponding to the neat crystalline form of Cysteine. The crystallinity of the Cysteine and the composites shows that a suitable inhibitor is used.

3.1.2 Morphological Study of PVPC, and PVPC by SEM-EDX

Figure 3 represents the surface chemistry and morphology of pure PVP (a) and pure cysteine (b) molecules obtained from the SEM-EDS analysis, while Fig. 4a, b, and (c) show the SEM micrographs of PVPC obtained at the various addition ratios of Cysteine from 1, 3, and 5%, respectively. A change in the structures and chemistry could be identified due to the addition of Cysteine.

The surface chemistry (EDS) in Fig. 4 shows chemical components from both pure compositing molecules within the synthesized molecules. With an increase in the cysteine ratio, the percentage weight of sulphur in the PVPC also increased from 0.47 to 7.45 wt%. As for Nitrium, the content varies in a small range between 18.05 and 19.4 wt%, whereas the percentage weight of carbon declines in a range of 30 to 25.79 wt% as cysteine ratios increase. The observation could be attributed to the polymerization process between PVP and Cysteine leading to the PVPC molecule.

3.2 Corrosion Evaluation of the Composite

In order to evaluate the protection efficiency of the synthesized polymer, parameters such as the effect of inhibitor concentration, the effect of immersion time, and temperature were investigated. The effect of concentration was studied to determine the optimal concentration for efficient protection of the mild steel. The effect of immersion time of the water-soluble PVPC was also investigated to establish the optimal exposure time leading to maximum protection. The effect of temperature provided insight into the impact of the temperature of the corroding environment on the inhibition efficiency. The gravimetric technique (ASTM Standard G1-03) is used to determine corrosion inhibition. The weight-loss

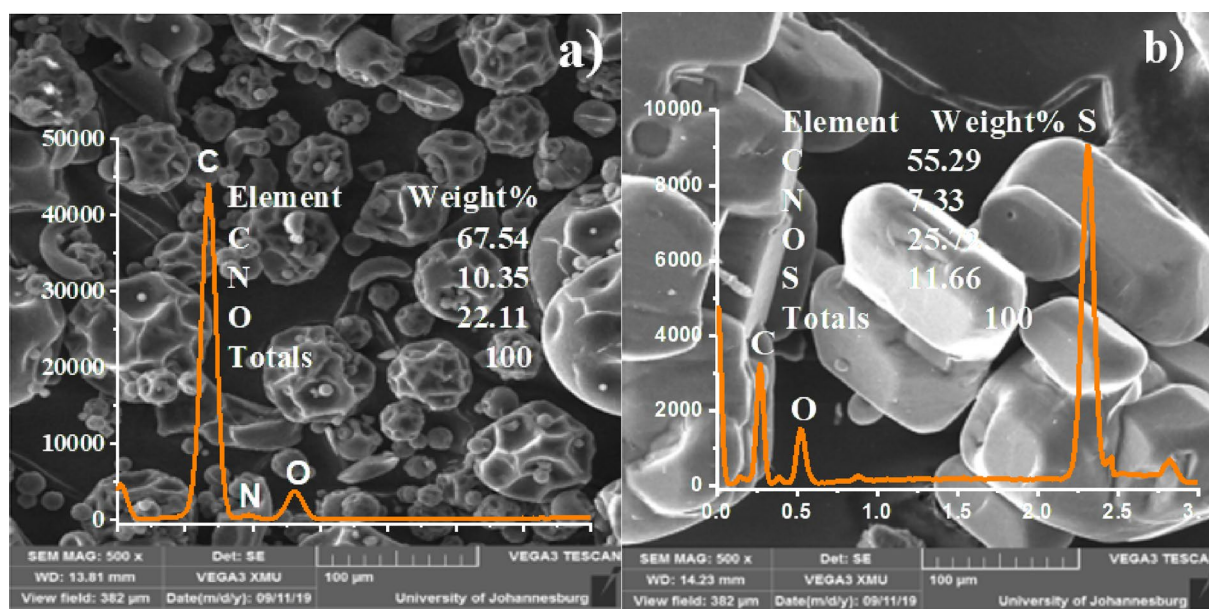


Fig. 3 SEM–EDX spectrum of pure PVP (a) and pure Cysteine (b)

method considered the effect of concentration, immersion time, and temperature on corrosion inhibition.

3.2.1 Effect of Concentration

Figure 5 summarizes the effect of the concentration of PVPC on corrosion inhibition at room temperature. Figure 5a–c details the corrosion rate of the MS in pure HCl solution and synthesized inhibitor. The optimization of the concentration effect on the corrosion rate and cysteine ratios is also determined. The corrosion rate, inhibition efficiency IE, and the effect of cysteine ratio were assessed under varying concentrations (25–800 ppm).

PVPC's dissolved mass increases with increasing concentration, resulting in an increase in protection efficiency from 18.4 to 85% across concentrations, while the corrosion rate decreases from 0.006 to 0.001 mg cm⁻² h⁻¹ as shown in Fig. 6a. The behaviour could be attributed to the presence of active adsorption sites on the mild steel surface, which allowed continuous interaction between the PVPC and the MS surface. The interaction is facilitated by some elements within the PVPC composite, such as N, S, and O [40]. While interacting with the mild steel surface, these atoms significantly mitigate the corrosion process as the concentration of PVPC increases [41, 42]. Above the 700 ppm concentration of inhibitor, a dropping trend of the protection efficiency is observed. The result could suggest a potential depletion of available active sites onto the metal surface to which inhibitors should adsorb themselves. It could also mean a probable desorption process occurring on the mild steel surface.

3.2.2 Effect of the Cysteine Ratio

The various ratios of Cysteine assessed at 500 and 700 ppm concentrations of inhibitor reveal a negligible impact on the inhibition efficiency. A relatively same protective efficiency is observed for the three respective cysteine ratios. The results suggested that the 1% ratio of Cysteine is optimum, and a further increase in cysteine to 3 and 5% did not have any effect on the protection efficiency. The findings are in line with those obtained by FTIR and XRD analysis. The latter had revealed a similarity in the molecular structures of the three PVPC molecules obtained from (10%) PVP and three different ratios of cysteine. Considering the current aspect of the results, only the (1%) PVPC is used for the rest of the experiments to minimize the inhibition cost [43, 44].

3.2.3 Effect of Immersion Time

The effect of immersion time at 25 °C from 3 to 24 h in 1.0 M of HCl is summarized in Fig. 6. For this investigation, five optimized inhibitor concentrations were used, which were 25, 100, 300, 500, and 700 ppm, respectively. The optimized parameters were attained after a series of experiments using different parameters. The results show an increase in the inhibition efficiency from 18 to 96.20%, with an exposure time increasing from 3 to 24 h as inhibitor concentration rises from 25 to 700 ppm. On the other hand, the corrosion rate decreases as the concentration and exposure time increase. This could suggest that an increase in the exposure time contributes to the adsorption mechanism of inhibitor molecules and, therefore, improves the inhibition

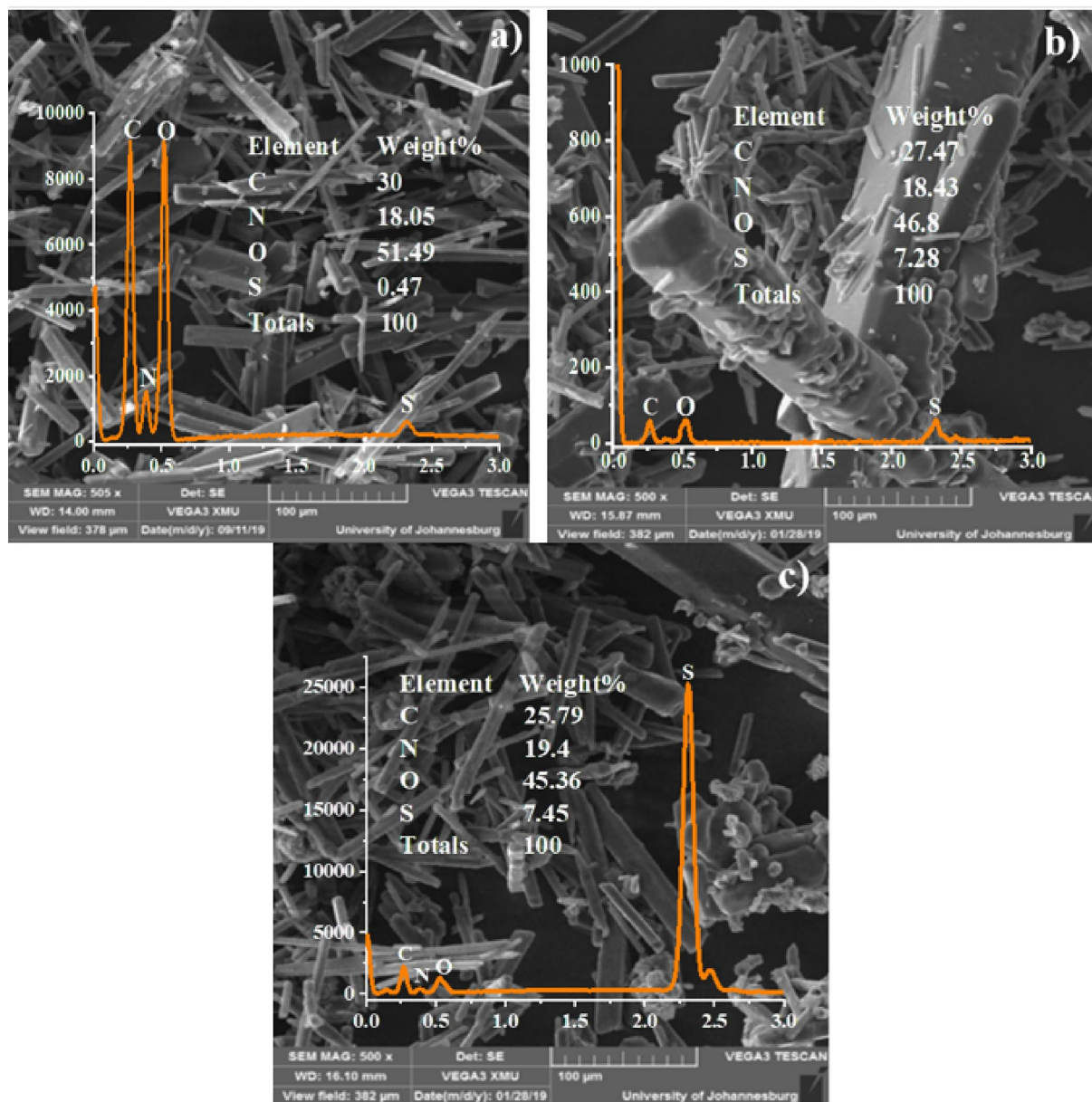


Fig. 4 SEM–EDX spectrum of a PVPC (1%), b PVPC (3%), and c PVPC (5%)

mechanism as the concentration of the inhibitor increases [45, 46].

Figure 6a shows an increasing trend of the corrosion rate for the blank solution as the immersion time increases and decreasing tendency as the concentration increases. It suggests the presence of a protective layer of inhibitor on the mild steel surface. The same results show a constant trend of the protection efficiency at 25 mg/L (25 ppm) concentration of PVPC for the immersion time range between 12 and 24 h. The trend suggests an interruption of both the adsorption and the oxidation processes. The interpretation given to this behaviour could correlate with the adsorption/desorption

equilibrium at the metal–solution interface [47, 48]. Furthermore, an equal inhibition efficiency for the two consecutive concentrations of PVPC (300 and 500 ppm) could be observed between 9 and 24 h. This behaviour indicates that the two concentrations inhibited the surface of mild steel in the same proportion by assuring the same surface coverage [49].

Table 3 shows the variation of the surface coverage (determined by Eq. 3) with the rise in the immersion time and the PVPC concentration. Considering the behaviour, therefore, we decided to consider the lower inhibitor concentration (300 ppm) instead of a higher concentration

Fig. 5 Effect of concentration of PVPC on **a** the corrosion rate of mild steel, **b** inhibition efficiency, and **c** influence of cysteine ratio of the inhibition efficiency

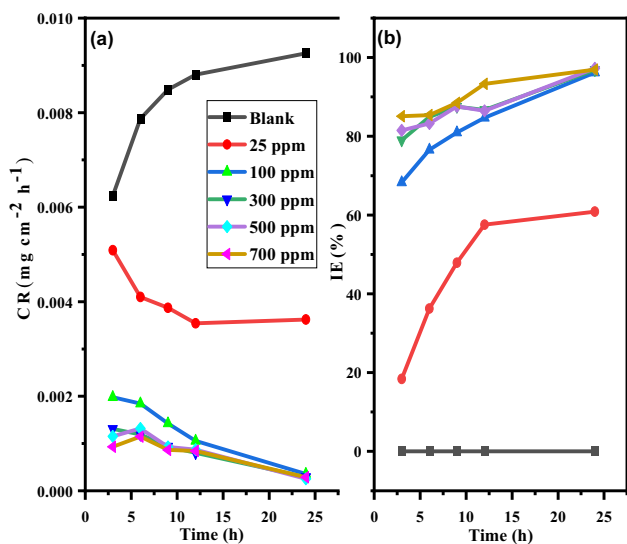
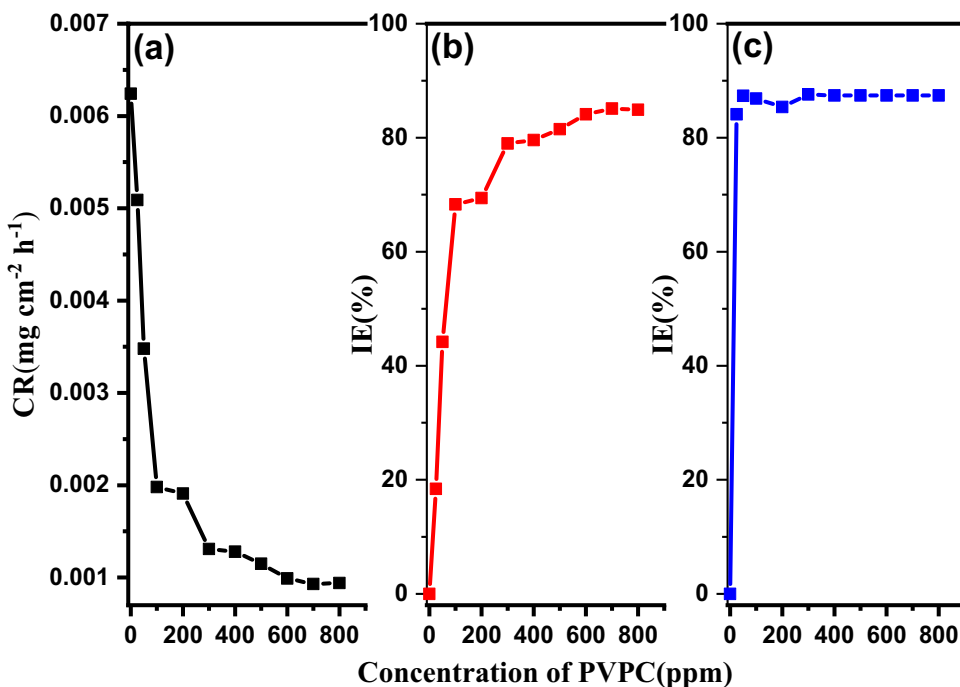


Fig. 6 Effect of immersion time on the corrosion rate of MS (a) and inhibition efficiency of PVPC (b)

(500 ppm) for economic and efficiency purposes [50, 51]. In addition, it is noticed that at 24 h, the variation of the inhibitor concentration does not affect the inhibition efficiency starting from 100 ppm, as shown in Table 3.

$$\theta = 1 - \frac{C_R}{C_{RO}} \tag{3}$$

where (θ) is the surface coverage; C_{RO} and C_R are the dissolution rates of mild steel exposed to an uninhibited and inhibited solution respectively.

3.2.4 Effect of Temperature

The effect of temperature is evaluated at 298, 303, 313, 323, and 333 K, respectively. The concentration of the inhibitor is also varied while the constant immersion time is maintained. The results in Fig. 7b revealed an increase in protection efficiency as temperature and concentration increase.

Table 3 Evolution of the fraction coverage with the increase of time and concentration

Time (h)	3		6		9		12		24	
	IE (%)	θ	IE (%)	θ	IE (%)	θ	IE (%)	θ	IE (%)	θ
25	18.4	0.18	36.27	0.36	47.90	0.48	57.6	0.58	60.9	0.61
100	68.3	0.68	76.60	0.77	80.98	0.81	84.7	0.85	96.2	0.97
300	79.0	0.79	84.90	0.85	87.54	0.88	86.7	0.87	96.9	0.97
500	81.5	0.82	83.24	0.83	87.60	0.88	86.5	0.86	97.3	0.97
700	85.1	0.85	85.40	0.85	88.48	0.88	93.3	0.93	97.0	0.97

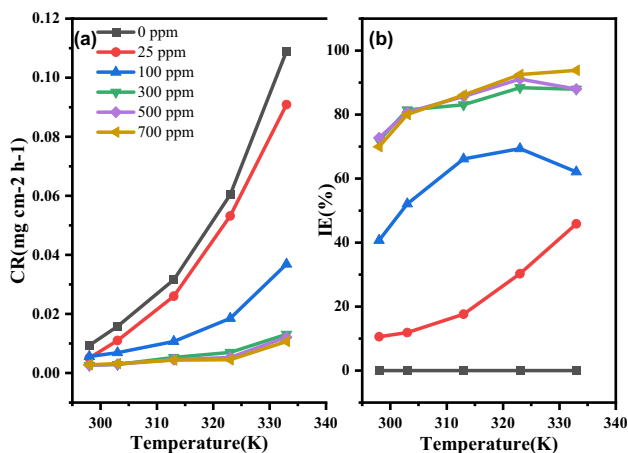


Fig. 7 Effect of temperature on the corrosion rate of MS (a) and inhibition efficiency of PVPC (b)

The optimum condition is reached at the 333 K and 700 ppm inhibitor concentration. The observation could suggest a chemisorption process as per previous reports made by researchers [52, 53]. Considering the findings, it can be assumed that temperature enhanced the adsorption process as it favours the inhibition kinetic. As expected, the rise in the corrosion rate of mild steel occurs as the temperature rises in the absence of inhibitor. In contrast, the increasing temperature decreases the corrosion rate of the mild steel when exposed to an inhibited electrolyte.

However, the usual trend of increasing protection efficiency is not detected for the concentrations 100–700 ppm at temperatures between 323 and 333 K. This behaviour could suggest the formation of solid and compact inhibitive layers already observed at 100 ppm. It also indicates that additional inhibitor atoms are unnecessary for the adsorption process [49]. Furthermore, it can be noticed from Fig. 7a that the temperature rises enhance the corrosion rate of the mild steel exposed to the uninhibited solution. However, the presence of inhibitors in the electrolyte facilitated the decrease in the corrosion rate [54, 55].

3.3 Kinetic and Thermodynamic Parameter

3.3.1 Kinetic Parameter

The sole kinetic parameter investigated in this section was the adsorption activation energy. This was determined to evaluate the concentration and temperature dependency of the corrosion inhibition. The values of the activation energy (E_a) for PVPC are shown in Table 4. At the same time, Fig. 8 is the linear plot of the mild steel corrosion rates versus the reciprocal of the experimental temperatures.

The results revealed a decrease in the activation energy with a rise in temperature and concentration of PVPC, as

Table 4 Activation energy of adsorption

Concentration (ppm)	E_a /KJmol ⁻¹
Blank	56.741387
025	66.370662
100	43.716675
300	37.470367
500	33.634287
700	27.787051

shown in Table 4. Such a finding agrees with the literature [40]. A previous interpretation for this observation is brought up by Riggs and Hurd [56], and Herrag et al. [57]. They assumed that the net dissolution reaction moves from the uninhibited bare part of the metal surface to the inhibited surface at the highest inhibitor concentration. In addition, the decreased activation energy with the increase in temperature for the inhibited solutions compared to that of the uninhibited solutions is demonstrated by [46, 58], and it is an indication of the chemisorption mechanism [59, 60]. The decrease in activation energy (E_a) suggested a more substantial contact between the adsorbate and the adsorbent's surface and promoted inhibited corrosion. A charge transfer mechanism between PVPC molecules and MS surfaces can also contribute to this phenomenon. This is also in line with the findings of Cordeiro et al. [61], where a higher temperature increases inhibition efficiency. The inhibition process is referred to as the substitution of water molecules by the inhibitor molecules on the MS surface [62, 63]. In addition, the decrease in activation energy with increasing inhibitor concentration could be explained by the fact that greater concentrations require less energy to displace water molecules from the surface of MS. The inhibitor concentration

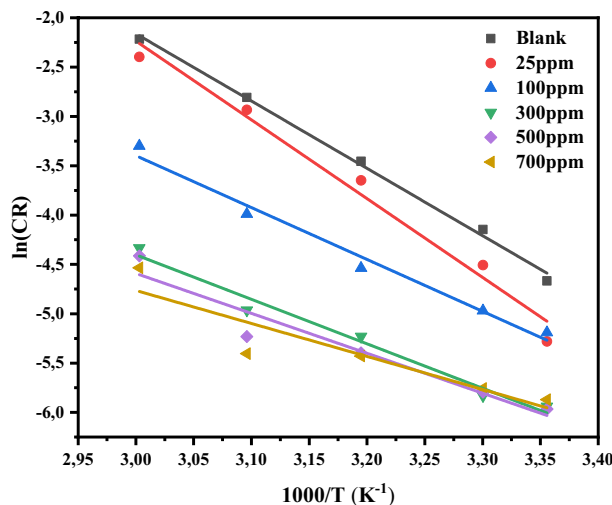


Fig. 8 Arrhenius plot for PVPC

facilitates the adsorption mechanism due to the higher activity of the inhibitor molecules [64].

3.3.2 Thermodynamic Parameters

The entropy, enthalpy, and Gibbs free energy of adsorption parameters are determined. These parameters provide insights into the temperature dependency (endothermic or exothermic) inhibition mechanism, the degree of the molecular disorder that the inhibition reaction generates, and the rate at which it is occurring (spontaneity or non-spontaneity).

3.3.2.1 Enthalpy and Entropy of Adsorption The calculated values of the enthalpy and entropy of adsorption are presented in Table 5.

From the results, the positivity measures the enthalpy of adsorption. Such positive enthalpies are reported to be indicative of an endothermic adsorption process, characterized mainly by heat consumption, while negative values of enthalpy were indicative of an exothermic adsorption process depicted by a heat release [65]. Moreover, it is reported that positive enthalpy adsorption is obtained for systems where significant protection efficiency is obtained with rising temperatures [66]. This can be interpreted as the adsorption mechanism of endothermic and stronger permanent contact that exists at higher temperatures between the inhibitor and MS [67]. Furthermore, the decreasing trend of the enthalpy of adsorption with the rise in both temperature and inhibitor concentration confirmed the adsorption of the PVPC on the mild steel substrate. This assumed that at a low temperature within an inhibited solution, the MS dissolution is faster compared to higher temperatures in the same inhibitor-containing solution.

However, the literature highlights that the entropy's sign of a system indicates whether the system entertains the disorder or not. A positive entropy indicates the presence of disorder within the system no matter the value [63]. It also implies the adsorbate affinity for the PVPC molecules in the adsorption mechanism, generating more translational energy than what is lost. Thomas [68] and Haque et al. [69] describe

it as endothermic chemisorption. From the results, it could be noticed that there is a decrease in the ΔS_{ads} values with rising temperature and concentration of the inhibitor [70]. This decrease in entropy of adsorption indicates that mild steel dissolution is characterized by significant molecular disorder at low temperatures and concentrations due to an interaction between the MS surface and the electrolyte. As the temperature and concentration of the inhibitor increase, the surface of mild steel becomes more and more covered by the inhibitor, which, therefore, inhibits the MS surface and lowers the molecular disorder consequently.

3.3.2.2 Adsorption Isotherms The Langmuir, Freundlich, and Temkin models of adsorption isotherm were used, and the model that best fitted the experimental data is adopted to determine the thermodynamic parameters (K_{ads} and ΔG_{ads}). The linear plots of adsorption isotherm models are shown in Fig. 9. The correlation coefficient (R^2) values of the three different adsorption isotherm models are presented in Table 5.

The regression coefficient should be closer to unity for the adsorption model to correlate with experimental data and indicate the nature of the formed inhibitive layer (monolayer or multilayer) [71]. Considering the values of the correlation coefficients shown in Table 6, it can be observed that only the Langmuir model best fitted the experimental data because of the regression coefficients (R^2) values found closer to unity at all temperatures. The results demonstrated that the polymer composite significantly interacted with the surface of the mild steel substrate to form a monolayer film of inhibitor.

The Temkin adsorption isotherm model also assumes a monolayer inhibitive film. The model presents regression coefficients closer to unity but lower than those from the Langmuir model [72]. However, the Freundlich adsorption isotherm model assumes a multilayer inhibitive film presented a correlation coefficient distant from unity [73]. Only the regression coefficient at the 303 K temperature seems closer to unity (0.92163). Therefore, based on these observations, it can be concluded that the adsorption mechanism of the PVPC obeyed the Langmuir adsorption isotherm.

3.3.2.3 Gibbs Free Energy of Adsorption The Gibbs free adsorption energy (ΔG_{ads}) details the reaction spontaneity as well as adsorption mechanism (physisorption or chemisorption). The Gibbs free adsorption energy was obtained from the adsorption–desorption equilibrium constant (K_{ads}), derived from the Langmuir adsorption isotherm, which best fitted the experimental data. The results of the Gibbs free energy of adsorption of the polymer composite and the adsorption equilibrium constant (K_{ads}) are shown in Table 7. From the results, an increase in the K_{ads} with an increase in temperature from 298 to 333 K could be observed. The

Table 5 Enthalpy and entropy of adsorption

Concentration (ppm)	$\frac{\Delta H_{\text{ads}}}{\text{KJmol}^{-1}}$	$\frac{\Delta S_{\text{ads}}}{\text{Jmol}^{-1}}$
Blank	54.1258	38.4644
25	63.7542	41.9949
100	41.1011	32.527
300	34.8548	29.2652
500	31.0187	27.6946
700	25.1715	25.5417

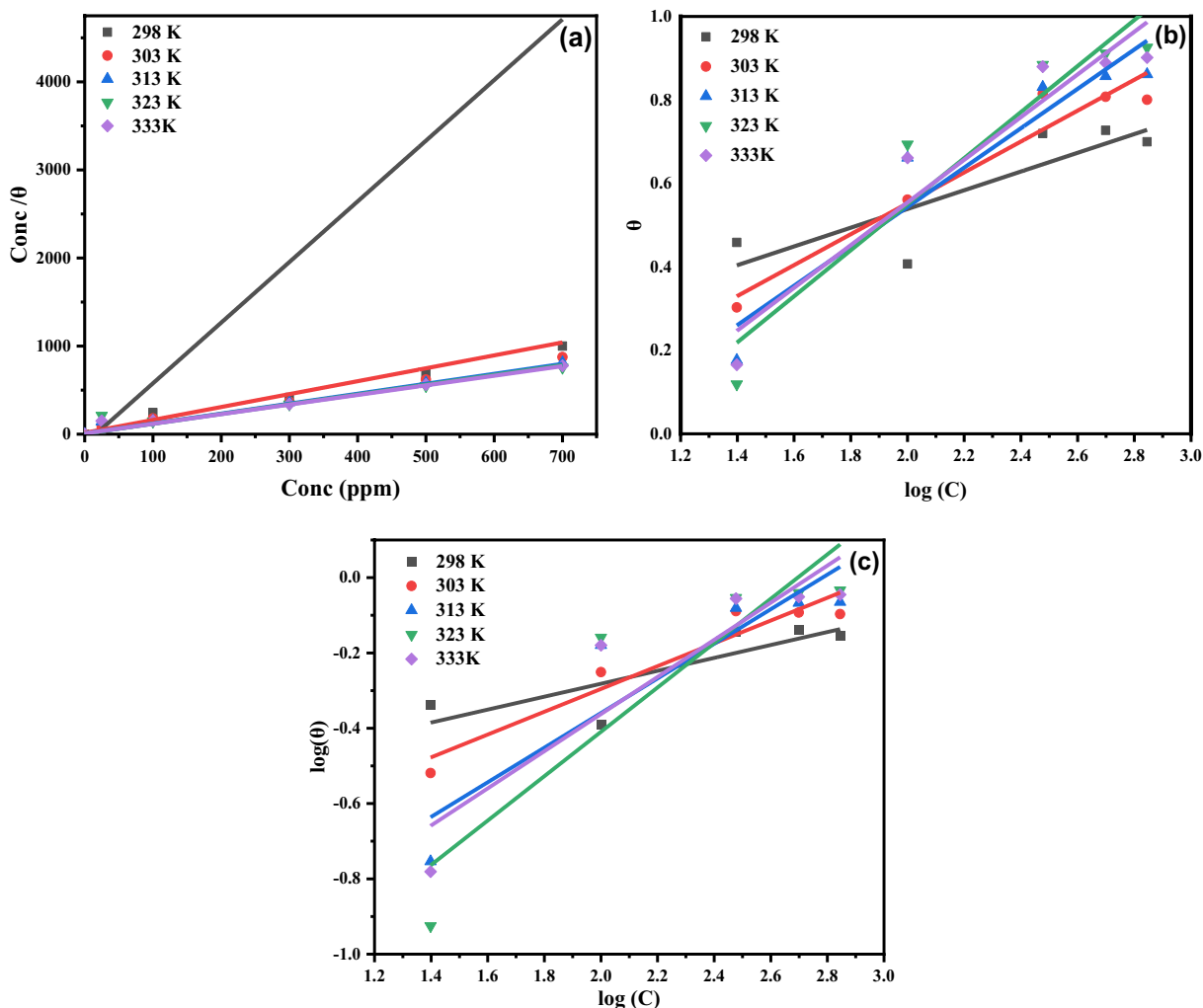


Fig. 9 Langmuir adsorption isotherm model (a), Temkin adsorption isotherm model (b), and Freundlich (c) at different temperatures

Table 6 Correlation coefficients for PVPC adsorption isotherm models

Temperature (K)	Correlation Coefficient (R^2) for various adsorption isotherm models		
	PVPC		
	Langmuir	Temkin	Freundlich
298	0.9433	0.71734	0.69413
303	0.9981	0.93926	0.92163
313	0.9993	0.90746	0.83162
323	0.9992	0.90520	0.81287
333	0.9982	0.91830	0.84024

behaviour suggested that the adsorption mechanism is temperature dependent since it is established that the more the temperature increases, the more the adsorption constant and the adsorption spontaneity increase. Such an increase in the

Table 7 Free Gibbs energy of adsorption for PVPC

Temperature(K)	Kads	ΔG_{ads} (KJ/mole)
298	0.647459	- 8.873876987
303	0.875427	- 9.782682997
313	1.27551	- 11.08501683
323	1.428776	- 11.74388972
333	2.379819	- 13.520.01647

adsorption equilibrium constant is also reported by Mert et al. [74], who ascribed the behaviour to the physisorption-adsorption mechanism.

The Gibbs energies of adsorption are found to be negative and lower than - 20 kJ/mole, which are also reported to be indicative of physisorption [75]. Therefore, the negative values of the Gibbs adsorption energy for PVPC can be ascribed to physisorption. However, the effect of

temperature investigated previously demonstrated the chemisorption adsorption mechanism of inhibitor on the surface of mild steel. The same observation was made with the decreasing activation energy values which are characteristics of a chemisorption inhibition mechanism between the PVPC and the steel surface [76]. Considering the actual discrepancy, it can be assumed that the adsorption mechanism obeyed both physisorption and chemisorption. Although, the physisorption showed dominance when referring to the values of the Gibbs adsorption energies.

3.4 Surface Analysis of Mild Steel

This section presents the surface analysis carried out on MS before and after the adsorption occurrence. The MS substrates were first exposed to an uninhibited solution and later immersed within an inhibited solution.

Figure 10a and b shows the surface of the as-received mild steel and corroded mild steel surface, respectively, while (c) shows a well-inhibited MS surface. The resistance of MS in inhibited solution to the corrosion process is relative to a compact inhibitor blanket on its surface. Such formation of an inhibitor layer can be associated with the change in surface roughness by comparison with the

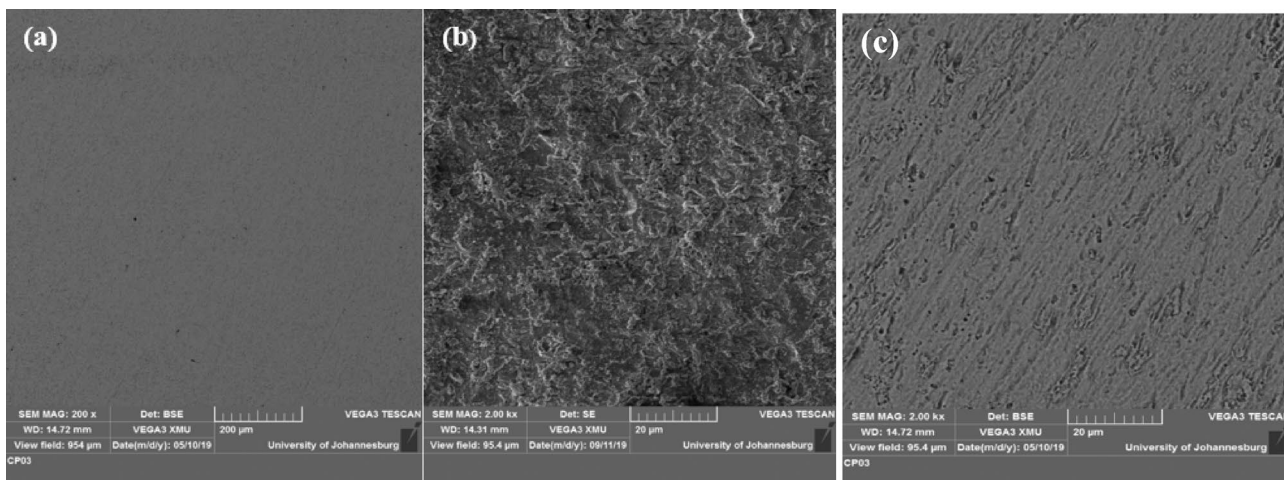


Fig. 10 SEM images for bare MS (a), MS exposed to 1 M HCl solution (b), and MS in 700 ppm-inhibited 1.0 M HCl solution (c)

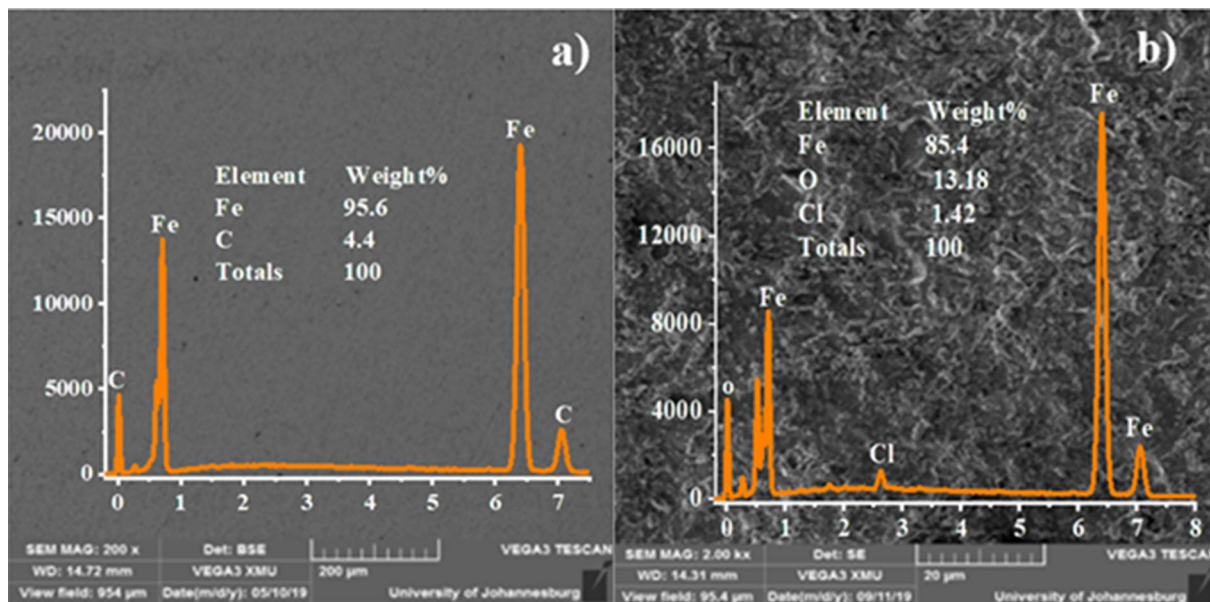


Fig. 11 EDX analysis of mild steel surfaces of a bare and b the corroded

surface roughness of the as-received mild steel, as shown in Fig. 11a. In addition to the surface analysis on bare, corroded, and inhibited mild steel using the SEM technique, the EDX analysis is also conducted on the as-received mild steel and the blank-immersed MS, respectively. The results were compared from a qualitative point of view.

From the findings in Fig. 11, the presence of chlorine and oxygen on the surface of the mild-corroded steel was noticed, while these elements were not present in the as-received sample. The observation suggested that the presence of chlorine and oxygen on the corroded mild steel substrate would come from the interaction between the MS surface and the 1.0 M HCl solution used as the electrolyte.

4 Conclusions

The present investigation aims to synthesize a new water-soluble and environmentally compatible compound or composite that is available as a polymer blend by compositing the polyvinylpyrrolidone with various concentrations and ratios of Cysteine. The following observations were made:

- (a) After synthesis and the polymerization of PVPC from (PVP) and (C), the cysteine ratios do not exhibit different characteristics such as structural and chemical properties as observed in results obtained from XRD, FTIR, and SEM
- (b) The corrosion evaluation involved weight-loss and surface analysis techniques. The study results revealed the invariance of the protection efficiency of PVPC with the variance in the concentration of cysteine in the PVPC molecule. The maximum protection efficiency of 85.1% is obtained from the optimal concentration of 700 ppm. It is also established that the protection capabilities increase with an increase in immersion time.
- (c) The thermodynamic response indicated the enthalpy of adsorption (ΔH_{ads}), the entropy of adsorption (ΔS_{ads}), and the Gibbs energy of adsorption (ΔG_{ads}). The calculated enthalpies were positively decreasing with the increase in temperature. This indicated that the adsorption process is energy depending and energy consuming (endothermic). Activation energy established that both chemisorption and physisorption occurred at the mild steel surface, but physisorption was dominant.
- (d) The SEM images after corrosion showed a robust inhibition efficiency of the PVPC inhibitor over bare mild steel and pure PVP inhibitor. The images also show a disparity in surface roughnesses that attests to a protective film.

Acknowledgements The authors would like to thank NRF for the financial support of this research. Also, we thank the University of Johannesburg for the research facilitation in terms of equipment and materials.

Funding All other authors certify that they have no affiliations with or involvement in any organization or entity with any financial interest or non-financial interest in the subject matter or materials discussed in this manuscript except C. K. Nsakabwe, who was on student bursary from the National research foundation of South Africa.

Data Availability The data are available with the authors and can be shared at any request.

Declarations

Conflict of interest The authors declare that there is no competing interest whatsoever regarding the publication of this article.

Ethical Standard All standards were duly followed.

References

1. Eddy NO, Odoemelam SA (2009) Inhibition of the corrosion of mild steel in H₂SO₄ by ethanol extract of aloe vera. *Resin Pigment Technol* 38(2):111–115
2. Alaneme K, Odoni U (2016) Mechanical properties, wear and corrosion behavior of copper matrix composite reinforced with steel machining chips. *Int J Sci Technol* 19:1593–1599
3. Hameed RSA (2011) Ranitidine drugs as non-toxic corrosion inhibitors for mild steel in hydrochloric acid medium. *Port Electrochim Acta* 29(4):273–285
4. Finšgar M, Jackson J (2014) Application of corrosion inhibitors for steels in acidic media for the oil and gas industry: a review. *Corros Sci* 86:17–41
5. Hameed RSA, Aljuhani EH, Al-Bagawi AH, Shamroukh AH, Abdallah M (2020) Study of sulfanyl pyridazine derivatives as efficient corrosion inhibitors for carbon steel in 10 m hcl using analytical techniques. *Int J Corros Scale Inhib* 9(2):623–643
6. Gerhardus H, Koch P, Michiel H, Virmani Y (2002) US report on corrosion costs and preventive strategies in the United States. Available: www.corrosioncost.com. Accessed 19 Jan 2019
7. Chigondo M, Chigondo F (2016) Recent natural corrosion inhibitors for mild steel: an overview. *J Chem* 2016:1–7
8. Faiza AZM, Awang K, Hussin H (2020) Corrosion inhibition on mild steel in 1 M HCl solution by *Cryptocarya nigra* extracts and three of its constituents (alkaloids). *R Soc Chem* 10:6547–6562
9. Saraswat V, Yadav M, Obot IB (2020) Investigations on eco-friendly corrosion inhibitors for mild steel in acid environment: electrochemical, DFT and Monte Carlo Simulation approach. *Colloids Surf A* 599:124881
10. Fayomi OSI, Olusanya D, Loto CA, Udoye NE (2021) Insight on the electrodeposition technology and parameter for corrosion control of structural steel. *IOP Conf Ser* 1036(1):012056
11. Umoren SA (2009) Polymers as corrosion inhibitors for metals in different media: a review. *Open Corros J* 2:175–188
12. Tsoenyane M, Makhatha M, Arotiba O (2019) Corrosion inhibition of mild steel by poly(butylene succinate)-L-histidine extended with 1,6-diisocyanohexane polymer composite in 1 M HCl. *Int J Corros* 20:4–85

13. Wilson K, Jawed M, Ngala V (2013) The selection and use of cathodic protection systems for the repair of reinforced concrete structures. *Constr Build Mater* 39:19–25
14. Mishra AK, Shoesmith DW (2014) Effect of alloying elements on crevice corrosion inhibition of nickel-chromium-molybdenum-tungsten alloys under aggressive conditions: an electrochemical study. *Corrosion* 70(7):721–730
15. Akinlabi ET, Baruwa AD, Oladijo OP, Maledi N, Chinn J (2019) Characterization of hydrophobic silane film deposited on aisi 304 stainless steel for corrosion protection. *J Mater Eng Perform* 28(10):6330–6339
16. Zhang QH, Hou BS, Li YY, Zhu GY, Liu HF, Zhang GA (2020) "Two novel chitosan derivatives as high efficient eco-friendly inhibitors for the corrosion of mild steel in acidic solution. *Corros Sci* 164:164
17. Haldhar R, Prasad D, Bhardwaj N (2020) Experimental and theoretical evaluation of acacia catechu extract as a natural, economical and effective corrosion inhibitor for mild steel in an acidic environment. *J Bio- and Tribo-Corros* 6:1–11
18. Chung I-M, Malathy R, Priyadharshini R, Hemapriya V, Kim S-H, Prabakaran M (2020) Inhibition of mild steel corrosion using *Magnolia kobus* extract in sulphuric acid medium. *Mater Today Commun* 25:1–11
19. Abdallah M, Fawzy A, Hawsawi H, Hameed RSA, Al-Juaid SS (2020) Estimation of water-soluble polymers (poloxamer and pectin) as corrosion inhibitors for carbon steel in acidic medium. *Int J Electrochem Sci* 15:8129–8144
20. Hameed RSA, Ismail EA, Al-Shafey HI, Mohamed AA (2020) Expired indomethacin therapeutics as corrosion inhibitors for carbon steel in 10 M hydrochloric acid media. *J Bio- Tribo-Corros* 6(4):1–10
21. Loto RT, Loto CA, Popoola A (2012) Corrosion inhibition of thiourea and thiazole derivatives: a review. *J Mater Environ Sci* 5:885–894
22. Sambyal P, Ruhi G, Dhawan SK, Bisht BMS, Gairola SP (2018) Enhanced anticorrosive properties of tailored poly(aniline-anisidine)/chitosan/SiO₂ composite for protection of mild steel in aggressive marine conditions. *Prog Org Coat* 119:203–213
23. Qian BWJ, Zheng M, Hou B (2013) Synergistic effect of polyaspartic acid and iodide ion on corrosion inhibition of mild steel in H₂SO₄. *Corros Sci* 75:184–192
24. Abdallah M, Al-Gorair AS, Fawzy A, Hawsawi H, Hameed RSA (2021) Enhancement of adsorption and anticorrosion performance of two polymeric compounds for the corrosion of SABIC carbon steel in hydrochloric acid. *J Adhes Sci Technol* 40:1–19
25. Hameed RSA, Aljohani MM, Essa AB, Khaled A, Nassar AM, Badr MM, Al-Mhyawi SR, Soliman MS (2021) Electrochemical techniques for evaluation of expired megavit drugs as corrosion inhibitor for steel in hydrochloric acid. *Intl Jf Electrochem Sci*. 16:1–12
26. Hameed RSA, Al-bonayan AM (2021) Recycling of some water soluble drugs for corrosion inhibition of steel materials : analytical and electrochemical measurements. *J Optoelectron Biomed Mater* 13(2):45–55
27. Mora LV, Naik S, Paul S, Dawson R, Neville A, Barker R (2017) Influence of silica nanoparticles on corrosion resistance of sol-gel based coatings on mild steel. *Surf Coat Technol* 324:368–375
28. Nasouri K, Shoushtari AM, Mojtahedi MR (2015) Effects of polymer/solvent systems on electrospun polyvinylpyrrolidone nanofiber morphology and diameter. *Polym Sci Ser A* 58:747–755
29. Al-Juhaiman LA (2016) Polyvinyl pyrrolidone as a Corrosion Inhibitor for Carbon Steel in HCl. *Int J Electrochem Sci* 11:2247–2262
30. Kurakula M, Rao GSNK (2020) Pharmaceutical assessment of polyvinylpyrrolidone (PVP): As excipient. *J Drug Deliv Sci Technol* 60:1–25
31. Layla A, Juhaiman A (2016) Polyvinyl pyrrolidone as a corrosion inhibitor for carbon steel in HCl. *Int J Electrochem Sci* 11(3):2247–2262
32. Al-Gorair AS, Hawsawi H, Fawzy A, Sobhi M, Alharbi A, Abdel Hameed RS, Wanees SA, Abdallah M (2021) Evaluation of the anticorrosion and adsorption properties of polyethylene glycol and polyvinyl alcohol for corrosion of iron in 10 M NaCl solution. *Int J Electrochem Sci* 16:1–16
33. Hameed RSA (2018) Cationic surfactant - zn+2 systems as mixed corrosion inhibitors for carbon steel in a sodium chloride corrosive medium. *Port Electrochim Acta* 36(4):271–283
34. Abdallah M, Fawzy A, Hawsawi H (2020) Maltodextrin and chitosan polymers as inhibitors for the corrosion of carbon steel in 10 M hydrochloric acid. *Int J Electrochem Sci* 15:5650–5663
35. Umoren S, Oguzie EE (2007) Corrosion inhibition of mild steel in 1 M H₂SO₄ by polyvinyl pyrrolidone and synergistic iodide additives. *Port Electrochim Acta* 26(6):533–546
36. Lyanage PD, Weerathunge P, Sing M, Bansal V, Ramanathan R (2021) L-Cysteine as an irreversible inhibitor of the peroxidase-mimic catalytic activity of 2-dimensional Ni-based nanozymes. *Nanomaterials* 11(5):1285
37. Anwar M, Pervaiz F, Shoukat H, Noreen S, Shabbir K, Majeed A, Ijaz S (2021) Formulation and evaluation of interpenetrating network of xanthan gum and polyvinylpyrrolidone as a hydrophilic matrix for controlled drug delivery system. *Polym Bull* 78(1):59–80
38. Saravanakumar K, Hu X, Chelliah R, Oh D-H, Kathiresan K, Wang M-H (2020) Biogenic silver nanoparticles-polyvinylpyrrolidone based glycerosomes coating to expand the shelf life of fresh-cut bell pepper (*Capsicum annum* L. var. *grossum* (L.) Sendt). *Postharvest Biol Technol* 160:111039
39. Tobby M, Brown J, Dennis A, Fakes M, Gao Q, Gamble J, Khimyak Y, McGeorge G, Patel C, Sinclair W, Timmins P, Yin S (2009) Amorphous drug-PVP dispersions: application of theoretical, thermal and spectroscopic analytical techniques to the study of a molecule with intermolecular bonds in both the crystalline and pure amorphous state. *J Pharm Sci* 98(9):3456–3468
40. Umoren SA, Ebenso EE (2008) Blends of polyvinyl pyrrolidone and polyacrylamide as corrosion inhibitors for aluminium in acidic medium. *Indian J Chem Technol* 44:355–363
41. Benabdellah M, Yahyi A, Dafali A, Aouniti A (2011) Corrosion inhibition of steel in molar HCl by triphenyltin-2-thiophene carboxylate. *Arab J Chem* 4(3):243–247
42. Espartero JC (2015) Polymeric materials for corrosion protection in geothermal systems. Case Western Reserve University
43. Tang J, Hu Y, Han Z, Wang H, Zhu Y, Wang Y, Nie Z, Wang Y (2018) Experimental and theoretical study on the synergistic inhibition effect of pyridine derivatives and sulfur-containing compounds on the corrosion of carbon steel in CO₂-saturated 35 wt.% NaCl solution. *Molecules* 23(12):14
44. Okafor PC, Zheng Y (2009) Synergistic inhibition behaviour of methylbenzyl quaternary imidazoline derivative and iodide ions on mild steel in H₂SO₄ solutions. *Corros Sci* 51:850–859
45. Sabirneeza AAF, Geethanjali R, Subhashini S (2015) Polymeric corrosion inhibitors for iron and its alloys: a review. *Chem Eng Commun* 202(2):232–244
46. Kanagavalli K, Sathyariya T, Rathika G (2014) *Caesalpinia pulcherrima* as corrosion inhibitor for mild steel in acid medium. *Int J Sci Eng Res* 5(10):1411–1416
47. Y. Ding, B. Brown, D. Young, S. Nestic and M. Singer (2017) Effect of temperature on adsorption behavior and corrosion inhibition performance of imidazoline-type inhibitor. In NACE International Corrosion Conference and Expo, Houston
48. Fiori-Bimbi MV, Alvarez PE, Vaca H, Gervasi CA (2015) Corrosion inhibition of mild steel in HCl solution by pectin. *Corros Sci* 92:192–199

49. Karthik G, Sundaravadevelu M (2016) Studies on the inhibition of mild steel corrosion in hydrochloric acid solution by atenolol drug. *Egypt J Pet* 25(2):183–191
50. Rahuma M, El-Sabbah M, Hamad I (2013) Effect of serine and methionine on electrochemical behavior of the corrosion of mild steel in aqueous solutions. *Int Schol Res Not* 14(1–7):2013
51. Rahuma MN, Kannan B (2014) Corrosion in oil and gas industry a perspective on corrosion inhibitors. *J Mater Sci Eng* 3:1–12
52. Popova A (2007) Temperature effect on mild steel corrosion in acid media in presence of azoles. *Corros Sci* 49:2144–2158
53. Okafor P, Ebenso E, Ekpe U (2004) Inhibition of the acid corrosion of aluminium by some derivatives of thiosemicarbazone. *Bull Chem Soc Ethiop* 18(2):181–192
54. V. G. Vasudha and. K. S. Priya, (2014) Corrosion inhibition of mild steel in H₂SO₄ media using polyalthia longifolia leaves. *Chem Sci Rev Lett* 2(6):435–443
55. Anbarasi K, Vasudha VG (2014) Corrosion inhibition potential of cucurbita maxima plant extract on mild steel in acid media. *Chem Sci Rev Lett* 3(9):45–51
56. Riggs OL Jr, Hurd RM (1967) Temperature coefficient of corrosion inhibition. *Corrosion* 23(8):252–1967
57. Herrag L, Hammouti B, Elkadiri S, Aouniti A, Jama C, Vezin H, Bentiss F (2010) Adsorption properties and inhibition of mild steel corrosion in hydrochloric solution by some newly synthesized diamine derivatives: Experimental and theoretical investigations. *Corros Sci* 52:3042–3051
58. Mraied H, Wang W, Cai W (2019) Influence of chemical heterogeneity and microstructure on the corrosion resistance of biodegradable WE43 magnesium alloys. *J Mater Chem B* 41:57
59. Eduok UM, Khaled MM (2014) Corrosion protection of steel sheets by chitosan from shrimp shells at acid pH. *Cellulose* 21:3139–3143
60. Hazwan MH, Kassim MJ (2010) The corrosion inhibition and adsorption behaviour of uncariagambir extract on mild steel in 1M HCl. *Mater Chem Phys* 125:461–468
61. Cordeiro RFB, Belati AJS, Perrone D, D'Elia E (2018) Coffee husk as corrosion inhibitor for mild steel in HCl media. *Int J Electrochem Sci* 13:12188–12188
62. Verma C, Pallikonda G, Chakravarty M, Quraishi M, Bahadur J, Ebenso E (2015) Aryl sulfonamidomethyl phosphonates as new class of green corrosion inhibitors for mild steel in 1M HCl: electrochemical, surface and quantum chemical investigation. *J Mol Liq* 209:51–59
63. Mohsenifar F, Jafari H, Sayin K (2016) Investigation of thermodynamic parameters for steel corrosion in acidic solution in the presence of N, N'-Bis(phloroacetophenone)-1,2 propanediamine. *J Bio Tribo Corros* 2(1):46
64. Mobin M, Zehra S, Parveen M (2016) L-cysteine as corrosion inhibitor for mild steel in 1M HCl and synergistic effect of anionic, cationic and non-ionic surfactants. *J Mol Liq* 216:598–607
65. Dabrowski A (2001) Adsorption - from theory to practice. *Adv Colloid Interfa Sci* 93:135–224
66. Mahgoub M, Al-Nowaiser FM, Al-Sudairi AM (2011) Effect of temperature on the inhibition of the acid corrosion of steel by benzimidazole derivatives. *Protect Metals Phys Chem Surf* 47(3):381–394
67. Jafari H, Akbarzade K, Danaee I (2014) Corrosion inhibition of carbon steel immersed in a 1 M HCL solution using benzothiazole derivatives. *Arab J Chem* 12:1387–1394
68. Thomas JM (1961) The existence of endothermic adsorption. *J Chem Educ* 38(3):138–139
69. Haque E, Won Jun J, Talapaneni SN, Vinu A, Jung SH (2010) Superior adsorption capacity of mesoporous carbon nitride with basic CN. *J Mater Chem* 20:10801–10803
70. Hameed RSA, Al-Bagawi AH, Shamroukh AH, Hassan AS, Abdallah M (2020) Corrosion Inhibition and Adsorption Properties of Some Heterocyclic Derivatives on C-Steel Surface in HCl. *J Bio-Tribo-Corros* 6(2):1–11
71. Rao HJ, King P, Kumar YP (2018) Equilibrium isotherm, kinetic modeling, and characterization studies of cadmium adsorption in an aqueous solution by activated carbon prepared from bauhinia purpurea leaves. *RASAYAN J Chem* 11(3):376–1392
72. Christmann K (2010) Thermodynamics and kinetics of adsorption. *Exp Theor Methods Surf Sci* 4:78–95
73. Foo K, Hameed B (2010) Insights into the modeling of adsorption isotherm systems. *Chem Eng J* 156:2–10
74. Mert B, Yuce A, Kardas G, Yazici B (2014) Inhibition effect of 2-amino-4-methylpyridine on mild steel corrosion: experimental and theoretical investigation. *Int J Corros Sci* 85:287–295
75. Subramania A, Kalyanasundaram N, Sathiyapriya R, Muralidharan V, Vasudevan T (2004) Polymeric corrosion inhibitors-an overview. *Bull Electrochem* 20:49–58
76. Chigondo M, Chigondo F (2016) Recent natural corrosion inhibitors for mild steel: an overview. *J Chem* 14:1–7

Publisher's Note Springer Nature remains neutral with regard to jurisdictional claims in published maps and institutional affiliations.